Comparative Ground Motion Studies

USGS Award No.: 99HQGR0024

Final Report 1999 - 2000

R. B. Herrmann
Earthquake Center
Department of Earth and Atmospheric Sciences
Saint Louis University
3507 Laclede Avenue
St. Louis, MO 63103
TEL: 314 977 3120
FAX: 314 977 3117
Email: rbh@eas.slu.edu

Program Element I.1

Key Words: Western U. S., Utah, High-frequency ground motion

March 27, 2001

Summary

This work reports on the distance dependence of high frequency ground motion in the 1-16 Hz range and compares the New Madrid Seismic Zone, the Southern Great Basin, southern California and most recently Utah to other locations in the western U. S. The study during this grant used data collected by the University of Utah Seismograph Station system and focused on high frequency ground within Utah associated with the essentially north-south line of seismicity through the central part of the state.

The purpose of this ongoing study is to quantify the regional variation in high frequency earthquake ground motion in regions monitored by regional seismic networks.

The study provides the basic research required to refine current regional ground motion models used in national seismic hazard studies.

Introduction

This research is part of a long-term effort to use regional seismic network data to constrain high frequency ground motions. The driving motivation is the urgency to provide state-of-the-art ground motion scaling for probabilistic seismic hazard analysis and engineering design. The situation facing most of the United States is the low rate of earthquake activity so that neither local earthquake nor strong motion recordings exist in sufficient numbers to define needed ground motion scaling relations. In a few regions, which have been or are monitored by regional seismic networks, digital recordings of small earthquakes may exist but there may be no strong motion recordings. Strong motion data exist in sufficient number for development of predictive relations in a few locations of the western United States. The lack of an empirical data base of expected strong ground motions applicable to the entire United States, requires the judicious use existing world-wide data (Spudich *et al.*, 1999) to extrapolate to larger events or to different regions.

Fortunately there is an abundance of vertical component waveforms for small earthquakes in some parts of the United States, so that their study may provide some constraints on the regional extrapolation. The effort behind this comparative study is to extend a methodology developed for New Madrid, Missouri to other regions of the United States. To date, we have applied the methodology to the following regions:

Region	Seismic Network
New Madrid	Cooperative New Madrid Seismic Network Data PANDA
Southern Great Basin	USGS/DOE
Wasatch Front	University of Utah Seismograph Stations
Washington and Oregon	Pacific Northwest Seismic Network
Germany	German Regional Seismic Network
Italy	Portable deployments, MEDNET
Central Mexico	RSVM, UNAM

Some of the results of these studies are given in the following publications:

Jeon, Y. S. (2000). High Frequency Earthquake Ground Motion Scaling in Utah, *M. S. (Research) Thesis* Saint Louis University, St. Louis, MO 124 pp. http://www.eas.slu.edu/Theses/sooymsr.pdf

Malagnini, L., R. B. Herrmann, and K. Koch (2000). Ground motion scaling in Germany, *Bull. Seism. Soc. Am.* **90,** 1052-1061.

Malagnini, L., R. B. Herrmann and M. Di Bona (2000). Ground motion scaling in the Apennines (Italy), *Bull. Seism. Soc. Am.* **90,** 1062-1081.

Malagnini, L., and R. B. Herrmann (2000). Ground motion scaling in the region of the 1997 Umbria-Marche earthquake (Italy), *Bull. Seism. Soc. Am.* **90,** 1041-1051.

Ortega, R. (2000). High Frequency Ground Motion in Central Mexico: Site, Excitation and Attenuation, *Ph. D. Dissertation, Saint Louis University, St. Louis, Missouri.*

Raoof, M., R. B. Herrmann and L. Malagnini (2000). Attenuation and Excitation of Three-Component Ground Motion in Southern California *Bull. Seism. Soc. Am.* **89** 888-902.

Methodology

The analysis of a data set requires data preparation, regression and forward modeling. The following sections discuss these steps.

Data Preparation

Digital waveforms are acquired from the network. Each event may have 100 or more associated traces. Each trace is previewed to remove clipped or otherwise bad waveforms. The P- and S-times are picked, and the trace is corrected for instrument response to form a velocity time history in units of *m/sec*.

The traces are next bandpass filtered at a center frequency f_c by passing them through an 8-pole Butterworth high-pass filter with corner $f_c/\sqrt{2}$ followed by an 8-pole low-pass filter with corner $\sqrt{2}\, f_c$; the peak filter gain is adjusted to be 1.0. Several filtered trace characteristics are tabulated:

- peak filtered velocity (*m/sec*) following the S arrival,

- the signal duration, defined as the interval within which the integral of filtered velocity squared following the S arrival changes from 5% to 75% of the maximum,
- the RMS Fourier velocity spectra (*m*) of the waveform within the duration window between frequencies $f_c/\sqrt{2}$ and $\sqrt{2}\,f_c$,
- the signal energy in consecutive time windows following S, for use in a Hoshiba separation of scattering and intrinsic Q,
- application of random vibration theory (RVT) to the spectra of the signal within the duration window to estimate peak motion and 5% nd 95% bounds on the estimated peak motion,
- RMS signal level as a function of time for coda-Q analysis and signal-to-noise estimation.
- event and station identification

The purpose of the extensive tabulation is to preserve enough information to characterize the signal for later analysis. The use of such narrow band filters rather than the traditional damped single degree of freedom response spectrum requires comment. Although a 5% damped oscillator appears to be a sharp filter, it is not. Its output waveform depends upon the signal input duration and frequency content. A high frequency signal, compared to the filter frequency, sees only the flat part of the transfer function, and hence will have an output frequency content much higher than the filter frequency. The narrow band combination of Butterworth filters used here will yield a filtered waveform with frequency content close to the center frequency of the filter. Thus we are better able to characterize the propagation of one frequency component of the ground motion. To get around an exact definition of the frequency content of the filtered waveform, we will subsequently define a forward model that is constrained by synthetic motions passed through the same filters.

The other difficulty with the use of lightly damped oscillators as filters is that the scaling from small earthquake observations to large earthquake motions is non-linear because of the interplay of signal duration, signal frequency content and the oscillator in estimating peak-motions. This is less of a problem with the use of the narrow bandpass filters.

It is now obvious that the task is to characterize wave propagation by analyzing small earthquake motions so that we can use use RVT to estimate peak motions for large earthquakes and for the lightly damped oscillators used to define response spectra. To do this, only the Fourier spectra and the duration of the motion are required. These are the measurements that form the basis of the Atkinson and Boore (1995) model for eastern North America are the Fourier spectra and duration. We analyze and model *both* the Fourier velocity *and* the peak filtered velocity values instead. Our reason for this extra effort is that this recognizes the imperfections of both the data and the modeling process. The observed Fourier velocity spectra requires a determination of the duration, which we have found shows a lot of scatter; the observed filtered peak velocity values have no such uncertainty. RVT modeling of the peak filtered velocities, though, requires the duration value. Our forward model must thus agree with three sets of observations, Fourier spec-

tra, peak motion and duration, in the context of RVT modeling.

Observed Motions

Observed ground motion is a function of source, site and path. Unless non-linear ground motions occur at the site, these three factors are theoretically separable, and additive in a logarithmic sense. Thus the observed logarithm of ground motion, $A(r, f)$, can be written as

$$A_{jk}(r, f) = E_j(r_{ref}, f) + S_k(f) + D(r_{jk}, f), \tag{1}$$

where r is the hypocentral distance, f is the observed frequency, j is the source index, $1 \le j \le J$, k is the site index, $1 \le k \le K$, r_{ref} is a reference distance, and E, S and D are the excitation, site and distance functions.

The term excitation is used since the regression only defines the scaling of observed ground motions and nothing about the seismic source. Other studies, such as Atkinson and Silva (1997), define a Fourier acceleration spectrum at a reference distance of 1 km. To emphasize that we wish to stably characterize observations, we specifically note the use of a reference distance by the term r_{ref}. The reference distance r_{ref} is selected to be within the range of observed distances so that we interpolate within the data set rather than extrapolate beyond, to be far enough from the source that errors in source depth do not significantly affect hypocentral distance, and yet not so far that expected super-critically reflected crustal arrivals complicate the motion. For these reasons we use a reference distance of $r_{ref} = 40$ km for our studies.

It is hoped that simple wave propagation models will suffice to predict the $A_{jk}(f, r_{ref})$. Of course, there must be observations on both sides of this reference distance to avoid extrapolation of poor data sets.

The function $D(r)$ in (1) is approximated by piecewise linear segments with a condition of continuity. This interpolation function is often discussed in finite element texts (Huebner, 1974) and was used for ground motion scaling by Anderson and Lei (1994), Savage and Anderson (1995) and Harmsen (1997). Using this interpolation function, the $D(r)$ is described in terms of the values at L nodes as

$$D(r) = \sum_{l=1}^{L} D_l N_l(r).$$

The linear interpolation function, the $N_l(r)$ is non-zero in the range $r_l \le r \le r_{l+1}$ and $D(r_l) = D_l$ by definition. The choice of the nodes is made by examining the distribution of data with distance. Nodes are spaced to enclose a sufficient number of observations for a stable, smooth inversion.

By construction (1) is linear minimization problem in $J + K + L$ unknowns. However, it is singular unless constrained. The constraints used here are

a) $D(r_{ref}) = 0$, where $r_{ref} = 40$ km,

b) $\sum_k S_k(f) = 0$, and

c) $D(r)$ is smooth.

Constraints are added to the system of linear equations by adding additional rows in the linear algebra problem; these rows are heavily weighted. Anderson and Lei (1994) and Harmsen (1997) use a linearity constraint on $D(r)$ by requiring the numerical second derivative estimate to be zero. This is important if it is necessary to pass an acceptable distance function through a gap in distances. We apply the condition

$$D_{l-1} - 2D_l + D_{l+1} = 0.$$

Strictly speaking, this condition is only a linearity constraint if the r_l are evenly spaced. We use an unequal spacing to ensure a sufficient number of observations to define the distance function within a given data range and to permit greater sampling in regions of expected rapid change distance function. This condition is thus a linearity constraint in a mapped distance space for unevenly spaced data.

The site constraint b) is one of many possible. One could force hard rock sites to have a site term of zero. The site effect used here focuses on relative site effects, and has the consequence that common site effects are then mapped into the $E_j(r_{ref})$ term, which is another reason that we refer to this symbol as an excitation of observed data rather than as a source term. The $E_j(r_{ref})$ is now seen to represent a mean ground motion level at a distance of r_{ref} from the source. When three component data are available, this is constraint can be modified to apply to only the vertical or to the horizontal components only, with the other component for a station floating freely.

Other aspects of this model that must be understood before accepting the results of an inversion are related to tradeoffs between the excitation, site and distance terms. Two extreme examples illustrate the problems. If one event dominates a distance range, then there will be a tradeoff between the excitation for that event and the adjacent distance terms. This occurs if an event is separated by a distance of the network dimensions from a neighboring event and if the distribution of distance nodes is too dense. In another extreme example, if only one station appears at a narrow range of distances and if it has an anomalous response, then the $D(r)$ will be distorted by this station and a bias introduced in all other site terms because of constraint b).

In practice plotting the observation distances by event and by station is a good diagnostic for discarding events or for defining the distance nodes. The goal is that each station observe events over a wide range of distances overlapping those of other stations, and that the distance ranges of events overlap.

The regression is applied to each processed frequency to yield the $E_j(r_{ref}, f)$, $S_k(f)$ and $D(r_{jk}, f)$. The next step is to interpret these observations in terms of a predictive model.

Theoretical Fourier Velocity Spectra

An expression for the predicted Fourier velocity spectra for a frequency f and a distance r is

$$a(r, f) = s(f, \mathbf{M}_W) g(r) e^{-\pi f r / Q(f) \beta} V(f) e^{-\pi f \kappa} \tag{2}$$

where $a(r, f)$ is the Fourier velocity spectra, $s(f, \mathbf{M}_W)$ is the source excitation as a function of moment-magnitude, $g(r)$ is the geometrical spreading function, $Q(f)$ is the frequency dependent quality factor which equals $Q_0(f/1.0)^{\eta}$, Q_0 is the quality factor at 1.0 Hz, $V(f)$ is a frequency dependent site amplification, and κ controls site dependent

attenuation of high frequency.

A comparison of the regression parameters for the Velocity spectra to the terms of this formula shows the association:

$$10^{E} = s(f, \mathbf{M}_W) g(r_{ref}) e^{-\pi f r_{ref}/Q(f)\beta} \overline{V(f)} e^{-\pi f \bar{\kappa}} \tag{3}$$

$$10^{D} = \frac{g(r) e^{-\pi f r/Q(f)\beta}}{g(r_{ref}) e^{-\pi f r_{ref}/Q(f)\beta}} \tag{4}$$

$$10^{S_i} = \frac{V(f) e^{-\pi f \kappa}}{\overline{V(f) e^{-\pi f \kappa}}}, \tag{5}$$

where $\overline{V(f) e^{-\pi \kappa f}}$ is the network average site effect arising from constraint b).

Time domain modeling

RVT requires the signal duration in addition in addition to the predicted signal spectra at the site. We have found much scatter in our duration estimates because the observed signals are superimposed on ground noise and because we use an automatic procedure to determine it from each trace. The observed duration values are fit using the same linear interpolator used for distance:

$$T(r) = \sum_{l=1}^{L} T_l N_l(r),$$

but now the only constraint is that $T(r = 0\,\mathrm{km}) = 0$. RVT predictions depend on the signal duration which is assumed to be

$$T_S + T(r),$$

where T_S is the source contribution and $T(r)$ is the distance dependent wave propagation contribution to total duration. The justification for the $r = 0$ constraint is that we assume that the duration of small earthquakes used]in the study to be small and that the measured duration is relatively insensitive to event size of the small earthquakes. Predictions for larger earthquakes will use a sufficiently large T_S that overwhelms the $T(0km) = 0$ constraint at short distance. We used a $L2$-norm to determine the T_l node values, but should perhaps use an $L1$-norm fit used by Malagnini *et al* (2000).

Modeling

We use the following steps to model the observables of (1).

- Fit the Fourier velocity $D(r)$ in terms of $g(r)$ and $Q(f)$. We assume that the $Q(f)$ is independent of distance. Even with our typical range of filter frequencies between 1 and 16 Hz, the $e^{-\pi f r/Q(f)\beta}$ trades off with the $g(r)$ so that we can not uniquely determine either. We assume that the 1 Hz $D(r)$ is not strongly affected by the $Q(f)$ and use this as a guide to the choice of $g(r)$. The $g(r)$ is kept as simple as possible, e.g., with just a few nodes between 1 and 400 km. The spread in the $D(r)$ as a function of frequency at large distance is indicative of the value of η - there will be a large spread for small η and no spread for $\eta = 1$. It is not difficult to find an acceptable set of parameters.

- Test the $g(r)$ and $Q(f)$ choice and refine the $T(r)$ values by fitting the $D(r)$ for the filtered peak velocity. To do this, we assume a small $\mathbf{M}_W$, e.g., 3.0, for the event size to predict the $s(f, \mathbf{M}_W)$. Even though the source term will not divide out for the normalized $D(r)$ in the way that it did for the Fourier velocity spectra in (5), we assume that the source effect is effectively removed when looking at narrow bandpass filtered signals.

  The reason for this stage is to check the internal consistency of the $g(r)$, $Q(f)$ and $T(r)$ to explain both the distance dependence of the Fourier velocity and the peak filtered motions.

- Constrain the $\overline{V(f)e^{-\pi\kappa f}}$ term. Figure 1 shows the Fourier acceleration spectra at a distance of 1 km for 6 different moment magnitudes and five stress drops, from 10 to 400 bars (following Boore, 1983). We see that the stress drop does not affect the source spectra in the 1-16 Hz frequency band for the smallest event. Lacking detailed information about the moment magnitudes of these small events and the mean site specific $V(f)$, we presently use the parameter κ_{eff} in our modeling, where

$$e^{-\pi\kappa_{eff} f} \approx \overline{V(f)e^{-\pi\kappa f}} .$$

  This may seem odd mathematically, but since the $V(f)$ monotonically increases from 1.0 at low frequency to a fixed high frequency value, and since we have a limited frequency range to fit a logarithmic function, we assume that this approximation is in error by only a constant factor at most.

Regional Comparison

In this section we compare the parameterizations for six regions: New Madrid, Southern Great Basin, Southern California, Pacific Northwest, Utah eastern North America (Atkinson and Boore, 1995). The $g(r)$ for and the $T(r)$ are shown in Figures 2 and 3, respectively. Table 1 shows the values for $Q(f)$. The geometrical spreading functions were constrained to be r^{-1} for short distances, consistent with current usage in the western United States (Atkinson and Silva, 1997). Keeping in mind the tradeoff with between $g(r)$ and $Q(f)$, we see variations on the order of only $\sqrt{2}$ among the six regions. The curve for UTAH will be discussed later as one of two possible models. In eastern North America, the NMD (New Madrid) curve lies above that of AB95. The $Q(f)$ values of Table 1 show distinct regional variations.

Table 1. Regional Parameters

Code	Region	$Q(f)$	κ_{ref}
AB95	SE Canada	$680\,f^{0.36}$	0.000
NMD	New Madrid	$900\,f^{0.30}$	0.045
SGB	Southern Great Basin	$230\,f^{0.5}$	0.04
PNSN	Pacific Northwest	$160\,f^{0.65}$	0.04
UTAH	Wasatch Front	$150\,f^{0.65}$	0.045
SCAL	Southern California	$170\,f^{0.47}$	----

Figure 4 shows the modeled $D(r)$ for the Fourier velocity spectra. These smooth curves to fit the regression results within the error bounds of fit. These results are normalized at a distance of 10 km The color scheme is the same for each inset. (Note the

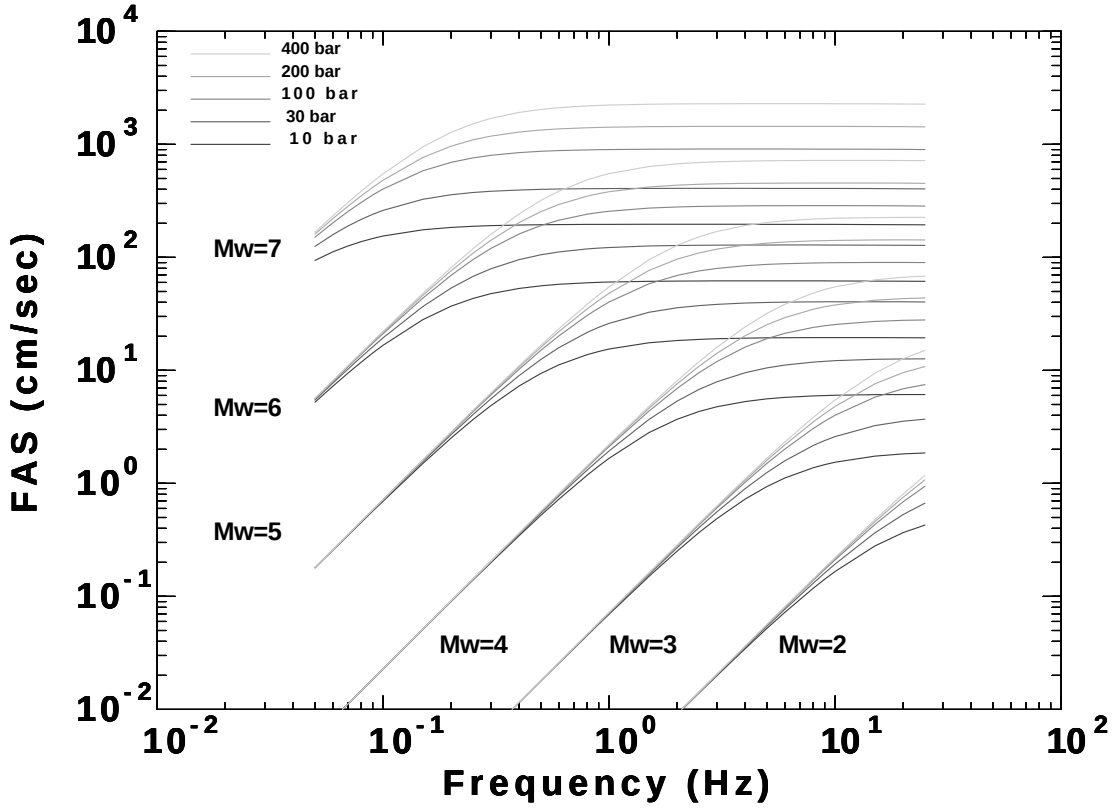

Fig. 1. Fourier acceleration spectra scaling $\mathbf{M}_W$ 2, 3, 4, 5, 6 and 7 and stress drop 10 bars (dark) to 400 bars (light). We use $\rho = 2.8$ gm/cm^3 and $\beta = 3.5$ km/sec, $H/V = 1$ and the Atkinson and Boore (1995) source spectral model with $\varepsilon = 1$ and the corner frequency relation $f_a 6 = f_b = 4.9 \cdot 10^6 \beta(\Delta\sigma/M_0)^{1/3}$.

Southern California has frequencies of 1 - 6 Hz because of the 20 Hz digital sampling rate of the data). The 1.0 Hz values, light gray, show distinct variations. For the same earthquake source input at 10 km, which will not be true because of regional differences in source spectrum scaling (Atkinson and Boore, 1998), we see that the New Madrid region would have the greatest expected motion at 300 km. We also that Utah uniformly has the lowest motions, especially in the 40 - 100 km distance range.

Figure 4 compares the normalized $D(r)$ for the peak ground velocities among the six regions. We again see that Utah has the lowest expected motions at all frequencies. We also not regional differences in the importance of the change in spreading due to the Moho arrivals.

Application to Large Earthquakes

The parameterization of ground motion can easily be incorporated into a random vibration theory (Boore, 1996). Several additional pieces of information are required:

- source scaling model, and
- correct site term, which should be compatible with our κ_{ref}

Figures 3, 4 and 5 indicate significant differences in the way individual frequency components of ground motion vary regionally. When considering large earthquakes, some of these differences may not be as important.

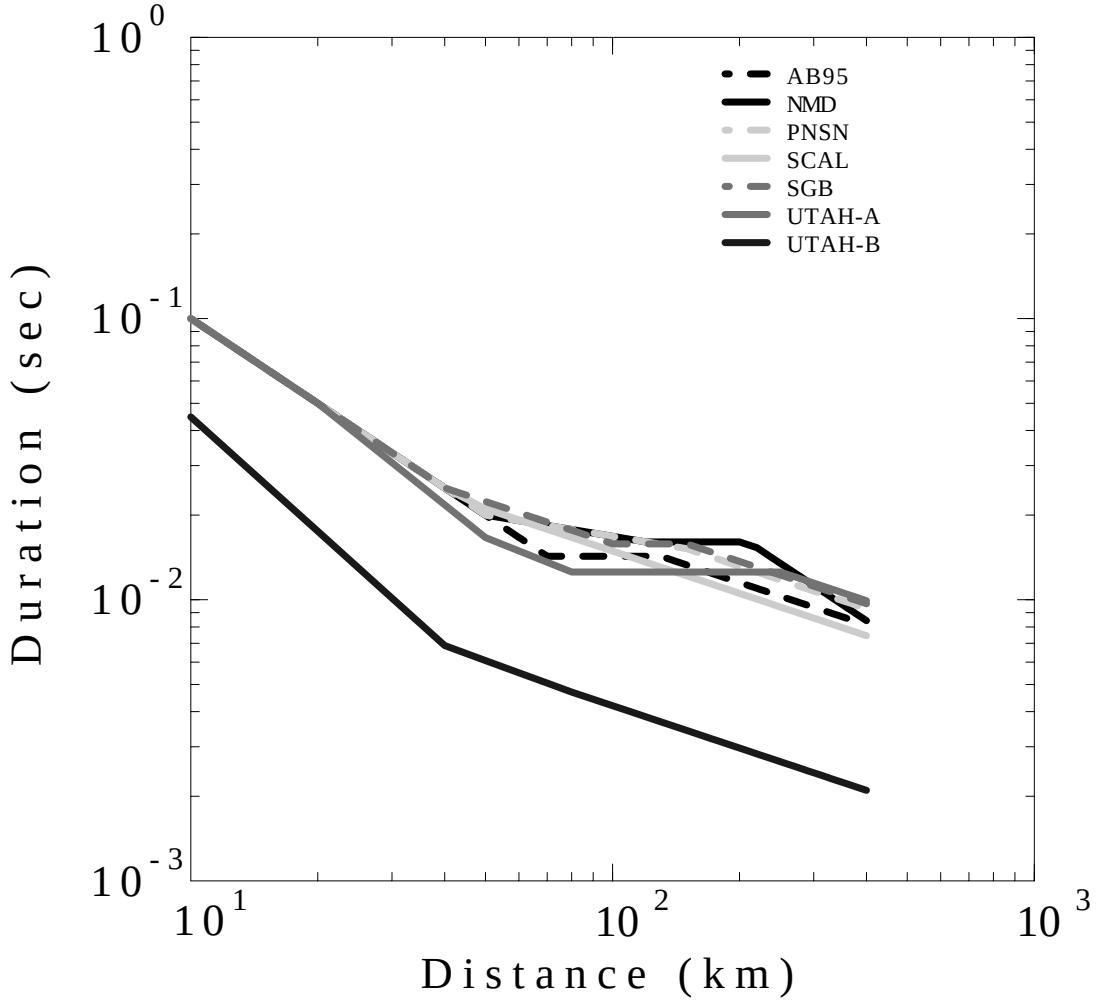

Fig. 2. Geometrical spreading function normalized at $r = 1$ km for the six regions. Two models for Utah are presented.

The differences in regional specific duration become less significant for larger earthquakes. This is because the peak motion is controlled by the total duration, $T_S + T(r)$, where Figure 3 presents our best estimate of the propagation duration. T_S for large earthquakes will be greater than the $T(r)$ at short distances, and thus will have a greater influence on the predicted peak motion.

Even though the propagation duration is less important for larger earthquakes, the regional differences in geometrical spreading, $g(r)$ and frequency dependent $Q(f)$ will continue to be important.

Recent Results and Insights from the Utah Data Set

Jeon (2000) processed 3000 waveforms from the University of Utah Seismograph Station archives from 279 events during the first 7 months of 1999. The data set was quite acceptable and led to some interesting surprises:

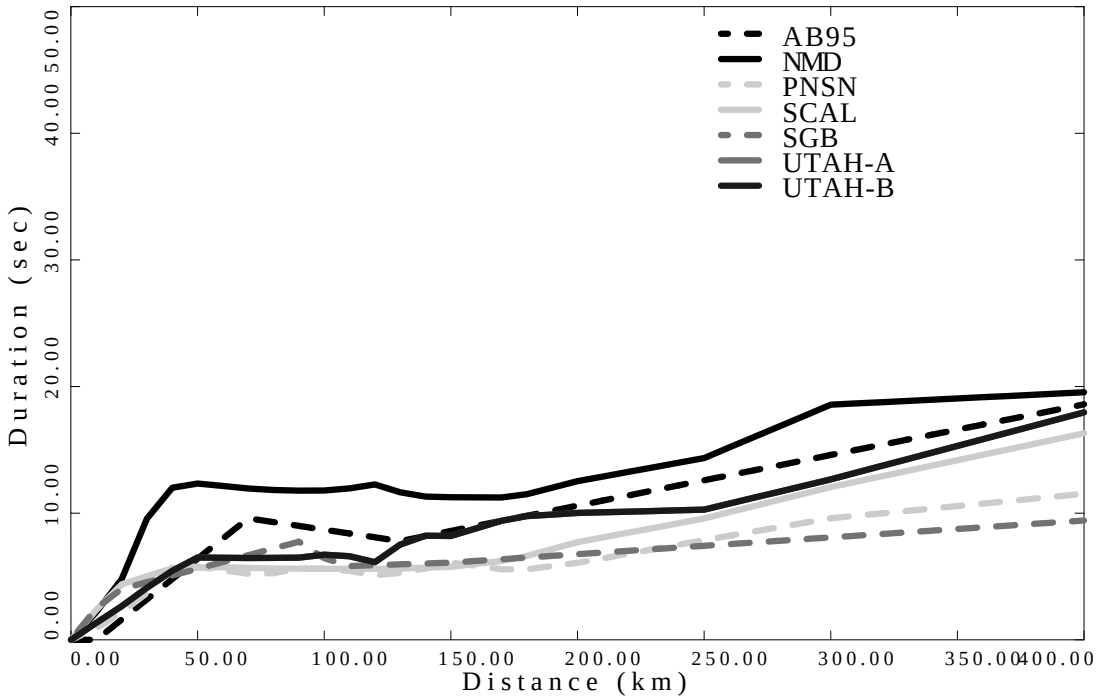

Fig. 3. Duration distance scaling for the six regions

• Rapid decrease of amplitude at short distance
• A corresponding strong tradeoff with the predicted excitation.

To model the observed $D(r)$, two models were constructed, A and B, that differed primarily in the geometrical spreading at short distances:

	Model A		Model B	
$Q(f)$	$145\,f^{0.65}$		$180\,f^{0.60}$	
$g(r)$	$r^{-1.0}$	$0 < r \le 20$	$r^{-1.35}$	$0 < r \le 40$
	$r^{-1.2}$	$20 < r \le 50$	$r^{-0.55}$	$40 < r \le 80$
	$r^{-0.6}$	$50 < r \le 80$	$r^{-0.50}$	$80 \le r$
	$r^{-0.0}$	$80 < r \le 250$		
	$r^{-0.5}$	$250 \le r$		
κ_{eff}	0.045		0.045	
$\Delta\sigma$	400	bars	400	bars

Figure 6 and 7 present the differences between the observed and model predicted peak filtered value $D(r)$ for Models A and B, respectively. The large deviations at high frequencies and $r > 200$ km are related to the reduced number of observations there. The large deviation at 125 km may be due to a poor instrument calibration or an artifact of the initial coda normalization $D(r)$ estimate (we will test the influence of the initial guess in a scheduled recomputation). However, sufficient observations exist between 20 and 40 km. Model B does fits the observed $D(r)$ better in this range of distances than does Model A. So the data require a rapid decrease of vertical component amplitude with distance. We

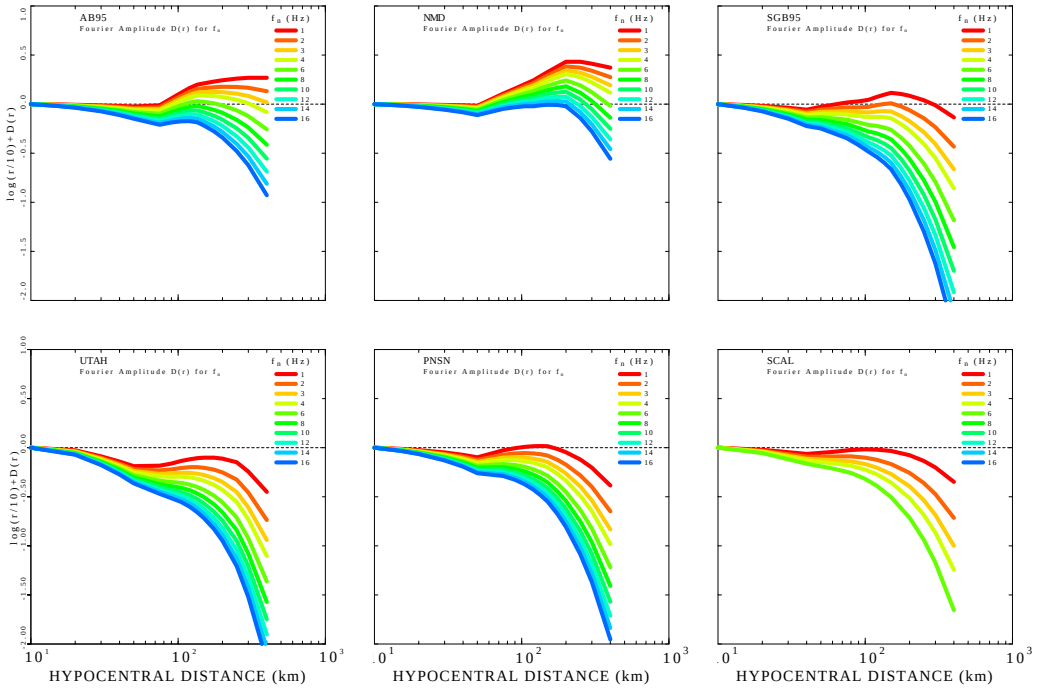

Fig. 4. Fourier velocity spectra distance scaling for the six regions, normalized at a hypocentral distance of 10 km

could have fit this using an r^{-1} trend and a very low $Q_0 < 100$, lower than anywhere else in the U. S.! Model A was constructed to have an r^{-1} at short distances, which is what is generally used in other studies, e.g., (Atkinson and Boore, 1995). The consequences of these two propagation models is very apparent when comparing the predicted to observed excitation $E(r_{ref}, f)$ in Figures 8 and 9, respectively for Models A and B, respectively. The procedure used was to focus on the small events, and to adjust the κ_{eff} so that the small predicted M_W values would parallel the observations. Hence the $\kappa_{eff} = 0.045$ sec. Then the stress drop was varied to attempt to match the shapes of the larger events using both log-log and log-lin plots. A $\Delta signal = 400$ bars was required since a lower stress drop would show the effect of corner frequency shift in the 1 - 16 Hz frequency range as the source sizes varies by the factor of 1000 of our data set.

The difference in the two propagation models is that Model A predicts motions about 0.5 $\log_{10}$ units larger at 40 km than Model B. The University of Utah $M_L's$ for the four largest events in these figures have $M_L's$ in the range 3.7 - 4.2 . To get a seismic moment, we compared some seismic moments from Nabelek

http://quakes.oce.orst.edu/moment-tensor/

to University of Utah $M_L's$ and found that $M_W \approx M_L$. This Model B seems to do a better job at predicting absolute levels, in spite of its very rapid geometrical decay at short distance.

So perhaps earthquake ground motions for Utah will be much lower than for other regions in the U. S. because of the rapid decrease of amplitude with distance. This has

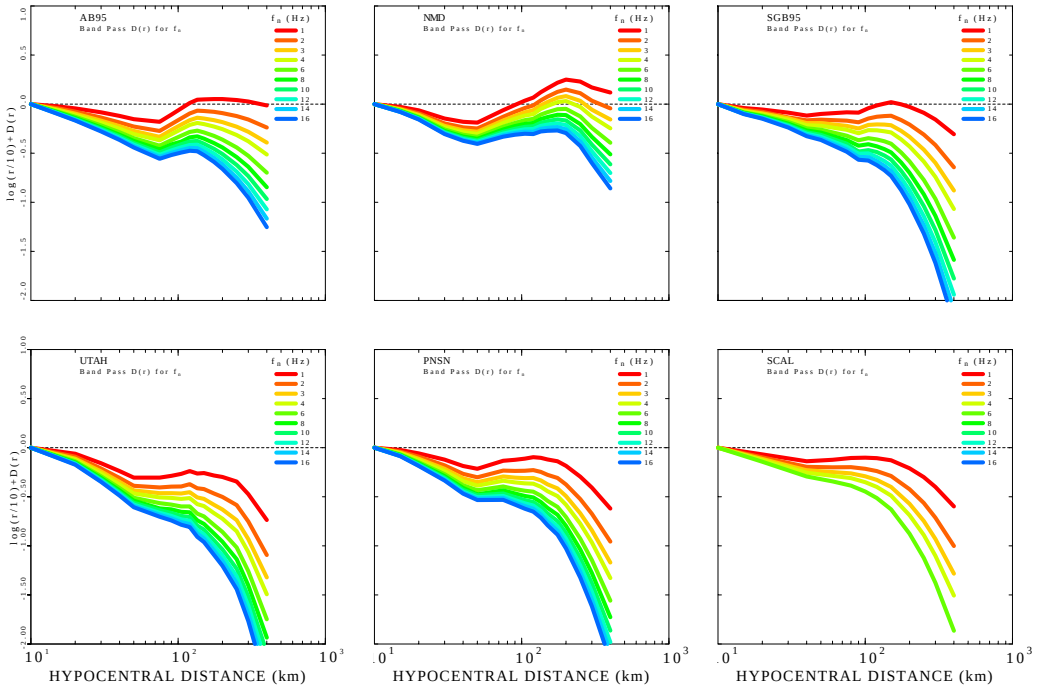

Fig. 5. Filtered velocity spectra distance scaling for the six region, normalized at a hypocentral distance of 10 km

major implications on expected ground motion for Utah earthquakes.

Discussion

The rapid decrease of high frequency ground motion in Utah decreases faster than the common assumption of R^{-1} geometrical spreading at short distances. This single result has significant consequences for current probabilistic ground motion hazard predictions if the controlling earthquakes are greater than 30 km from the site of interest because the data indicate a reduced level of motion. There may be a degree of conservatism in the current hazard maps; however the lack of knowledge in source scaling may introduce even more conservatism.

We are currently acquiring more data for the Utah-Wyoming region from the IRIS Data Management Center to focus on two important, but related questions. What is the geometrical spreading at short distances and are current source scaling laws adequate for the region. During the summer of 2001, Mr. Young-Soo Jeon will complete a paper on wave propagation in the region; this paper will be submitted to the Bulletin, Seismological Society of America.

References

Atkinson, G. M., and D. M. Boore (1995). Ground-motion relations for eastern North America, *Bull. Seism. Soc. Am.* **85,**

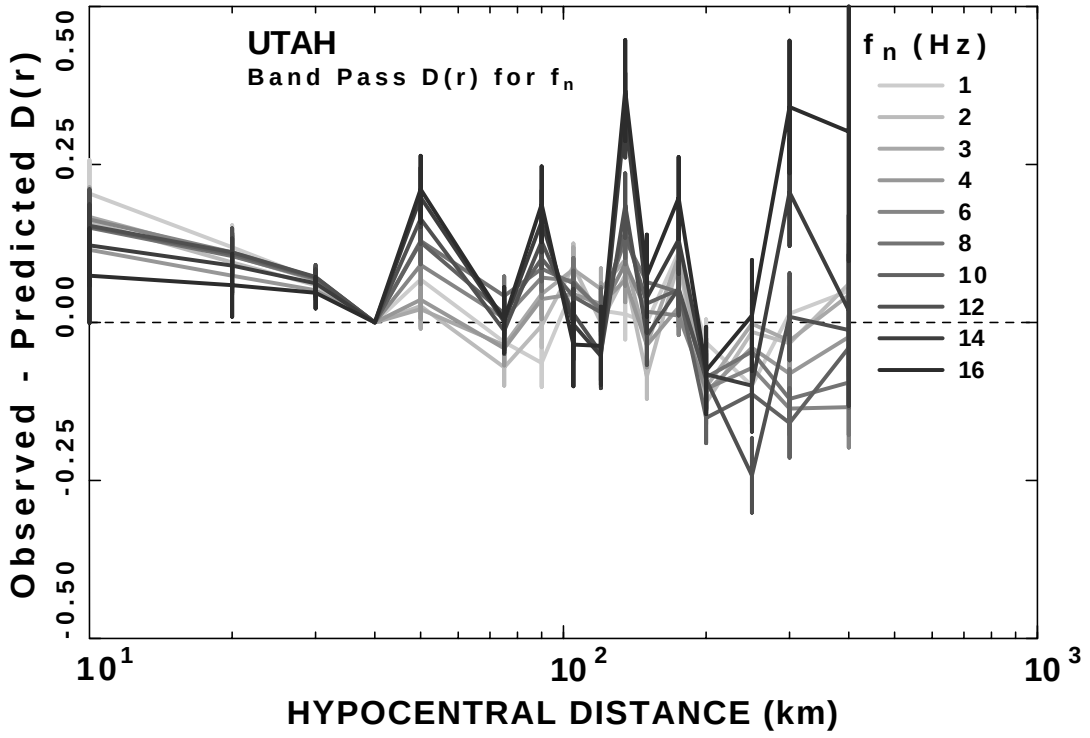

Fig. 6. Residuals of model fit to peak filtered velocity as a function of distance and frequency when using propagation model A. Differences are in $\log_{10}$ units. Note that at most distances and frequencies, predictions are within a factor of 1.6 90.2 log units) or better.

Atkinson, G. M., and W. Silva (1997). An Empirical study of earthquake source spectra for California earthquakes, *Bull. Seism. Soc. Am.*, 87 97-113.

Atkinson, G. M., and W. Silva (1997). An empirical study of earthquake source spectra for California earthquakes, *Bull. Seism. Soc. Am.* **87,** 97-113.

Boore, D. M. (1983). Stochastic simulation of high-frequency ground motions based on seismological models of the radiated spectra, *Bull. Seism. Soc. Am.* **73** 1865-1894.

Harmsen, S. (1997). Estimating the Diminution of Shear-Wave Amplitude with Distance: Application to the Los Angeles, California, Urban Area *Bull. Seism. Soc. Am.* 87 888-903. 17-30.

Savage, M. K., and J. G. Anderson (1995). A local-magnitude scale for the Western Great Basin - Eastern Sierra Nevada from synthetic Wood-Anderson seismograms, *Bull. Seism. Soc. Am.* **85,** 1236-1243.

Spudich, P., W. B. Joyner, A. G. Lindh, D. M. Boore, B. M. Margaris and J. B. Fletcher (1999). SEA99 - A revised ground motion prediction relation for use in extensional tectonic regimes, *Bull. Seism. Soc. Am.* **89,**, 1156-1170.

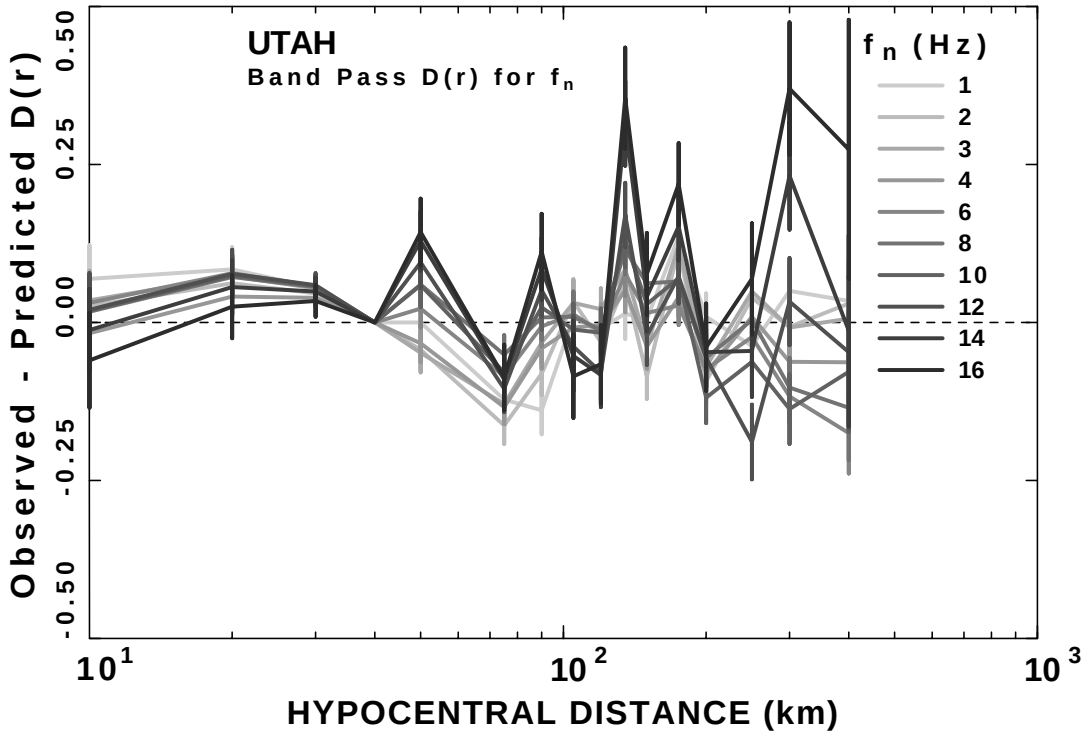

Fig. 7. Residuals of model fit to peak filtered velocity as a function of distance and frequency when using propagation model B. Differences are in $\log_{10}$ units.

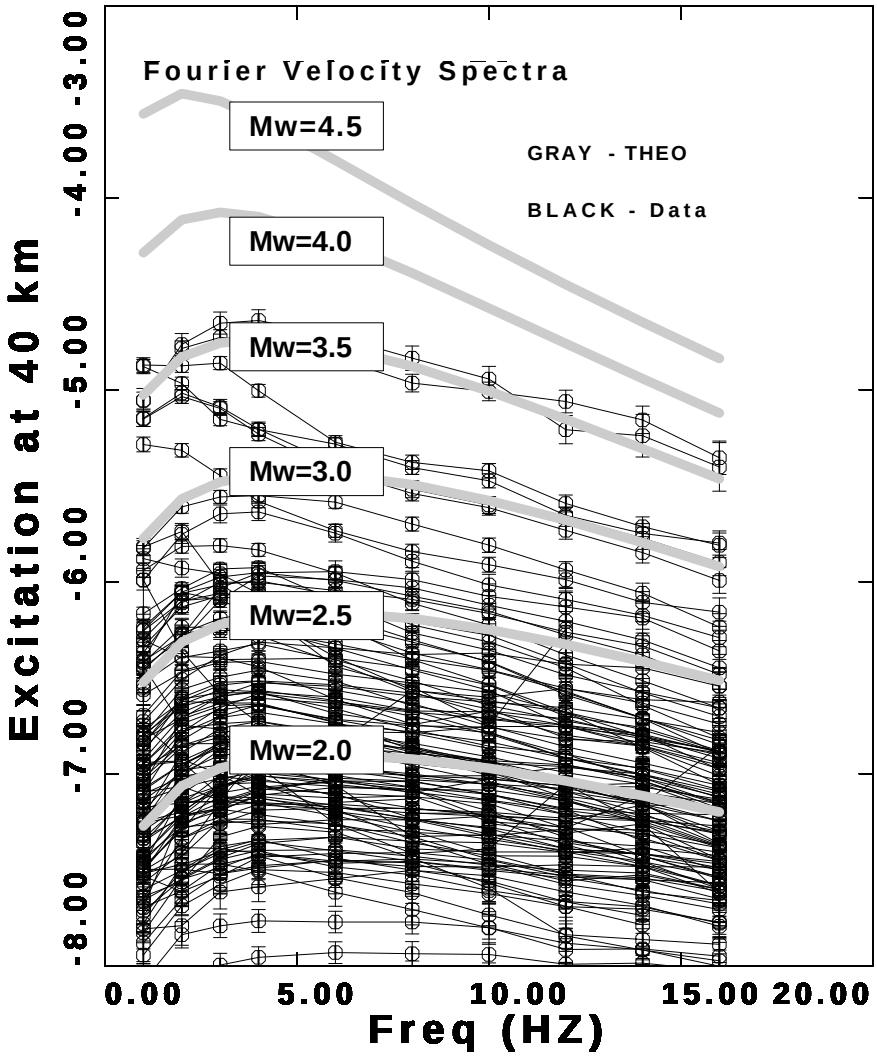

Fig. 8. Excitation of Fourier velocity spectra at 40 km for Model A. The thick gray curve is the prediction using a 400 bar stress drop. E is the $\log_{10}$ level of the Fourier velocity spectral amplitude in m.

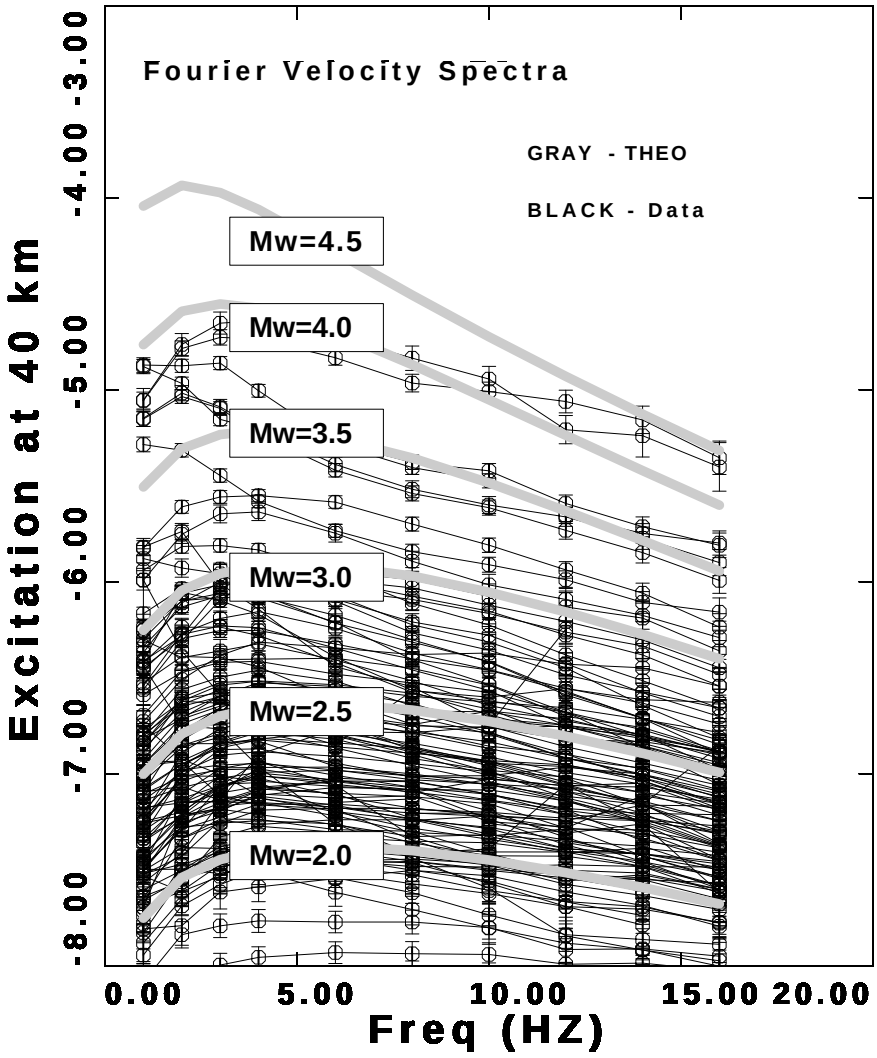

Fig. 9. Excitation of Fourier velocity spectra at 40 km for Model B. The thick gray curve is the prediction using a 400 bar stress drop. E is the $\log_{10}$ level of the Fourier velocity spectral amplitude in m.